Exploring Occupant Injury with Finite Element Reconstructions of Crash Injury Research and Engineering Network (CIREN) Motor Vehicle Crashes

C. G. Costa[1], A. A. Weaver[1], J. P. Gaewsky[1], F. S. Gayzik[1], J. D. Stitzel[1]
[1]Virginia Tech-Wake Forest Center for Injury Biomechanics

ABSTRACT

Two frontal Crash Injury Research and Engineering Network (CIREN) cases were reconstructed using finite element (FE) models. The interior of an exemplar vehicle was scanned for each case and individual parts of a FE simplified vehicle model (SVM) were transformed to align with the geometry of the exemplar interior scan. The simplified 50th percentile male Global Human Body Models Consortium (GHBMC) v1.8.4.1 human body model (HBM) was scaled to approximate the mass and height of the case occupant. The GHBMC model was then settled and belted in the transformed SVM using occupant positioning information obtained from the crash investigation. The SVM was subjected to the velocity pulse from the CIREN vehicle's event data recorder (EDR) and the belt pretensioner and airbag were set to trigger based on the EDR information. The occupant's injuries were compared with the occupant kinematics and injury metrics from each simulation and used to determine injury causation. The Murano case occupant sustained right 8th and 9th rib fractures and a sternal fracture. The Lexus case occupant sustained fractures of left ribs 3-5, 8, and 9 and a sternal fracture. Both reconstructions generated elevated strains in the local rib and sternum regions where fracture occurred in the CIREN occupants. Both reconstructions illustrated elevated strains in the ribs and sternum underneath the path of the belt restraint. Only strains in rib 9 and the sternum for the Lexus reconstruction surpassed fracture thresholds defined by Kent, et al. (2005), with values of 2.1% and 3.3%, respectively. Reconstructions were able to discern times of maximum belt restraint and airbag engagement, thereby allowing for greatly improved determination of injury causation in frontal collisions.

INTRODUCTION

Approximately 1.35 million people are killed in motor vehicle crashes (MVCs) annually worldwide and an additional 20-50 million people sustain non-fatal injuries (WHO, 2018). Although laboratory crash tests are an important aspect of motor vehicle safety testing, there are many factors they do not account for that are present in real-world crash scenarios. Additionally, anthropomorphic test devices (ATDs), while providing useful information about passenger kinetics and kinematics, are unable to assess organ-level injuries and occupants with a variety of different body morphologies and sizes (Shigeta, 2009). The Crash Injury Research and Engineering Network (CIREN) study seeks to fill these gaps by conducting detailed analyses of real-world crashes to determine injury causation and mechanism. For each CIREN case, data collection involves investigating the crash vehicle, crash scene, police records, and patient medical records with the goal of determining the cause of each injury the occupant sustains. However, even with the large sum of information present in each CIREN case, a significant amount of imagination is required to determine case occupant kinematics and injury causation.

Finite element (FE) analysis using human body models (HBMs) and adjustable vehicle models allows for the assessment and visualization of organ-level injury, bone strains, and occupant kinematics in a variety of different vehicle geometries and crash scenarios (Gaewsky, 2015; Hayashi, 2008; Ye, 2018). A few studies have reconstructed CIREN cases of frontal and side impacts using the Total HUman Model for Safety (THUMS) (Belwadi, 2012; Danelson, 2015; Gaewsky, 2015; Ye, 2018). However, these studies have reconstructed cases that, at the time, had already been reviewed to determine injury metrics or validate a model, not aid in the initial case review.

During CIREN case reviews, it is often difficult to imagine occupant kinematics and injury causation. For example, when reviewing frontal collisions involving rib and sternum fractures, it is difficult to determine how far forward the occupant moves and whether the fractures resulted more from contact with the seat belt or the steering wheel and airbag assembly. Sometimes, injury patterns may reveal extra information, such as a positive seatbelt sign or anterior rib fractures in the shoulder belt path (Crandall, 2000; Kallieris, 1998; Newman, 1984), but this is often not the case. This study sought to develop a rapid, but accurate, methodology for reconstructing a broad range of CIREN cases by reconstructing two CIREN frontal MVCs using an adjustable simplified vehicle model (SVM) and a HBM and comparing rib and sternum fractures in the case occupant to those in the HBM. The reconstructions were used during case reviews to assist in the determination of injury causation.

METHODS

Case Details

Two frontal CIREN cases (2014 Nissan Murano; 2013 Lexus ES350) were selected from the list of upcoming Wake Forest cases that were currently under investigation. Selection was limited to crashes with a principal direction of force (PDOF) between 340° and 20°, belted occupants, deployment of the steering wheel or knee bolster airbags only, an available event data recorder (EDR) report, and no driver compartment intrusion or rollover.

Nissan Murano Case Details. This case involved the driver of a 2014 Nissan Murano midsize sport utility vehicle (SUV). The occupant was a 61-year-old female who was 71 inches tall and weighed 180 lbs. The case vehicle struck the frontal plane of a compact SUV. The EDR report showed a delta-V of -28 mph in the longitudinal direction and -1 mph in the lateral direction, resulting in a PDOF of 0°. Only the steering wheel airbag deployed. The case occupant's seat was between the forward and middle track positions. She sustained a sternum fracture and fractures of right ribs 8-9.

Lexus ES350 Case Details. This case involved the driver of a 2013 Lexus ES 350 full size sedan. The occupant was a 66-year-old male who was 71 inches tall and weighed 165 lbs. The case vehicle struck the frontal plane of a Ford F-150 pickup truck. The EDR report showed a delta-V of -39.6 mph in the longitudinal direction and -3.3 mph in the lateral direction, resulting in a PDOF

of 10°. The steering wheel and knee bolster airbags deployed. The case occupant's seat was in the middle track position. He sustained a sternum fracture and fractures of left ribs 3-5 and 8-9.

Case Reconstructions

Reconstructions were conducted using a three-step process. The first step involved acquiring a 3D scan of an exemplar version of the case vehicle and rigidly transforming a FE SVM to best approximate the exemplar vehicle scan. The second step involved positioning and settling the 50th percentile male simplified Global Human Body Models Consortium (GHBMC) FE HBM into the vehicle model. The third step involved applying the EDR-reported delta-V velocity curve to the floor of the SVM to simulate the crash.

Step 1: Exemplar Scanning and SVM Transformation. An exemplar version of the case vehicle or a sister or clone of the case vehicle that had the same interior geometry was scanned using a Faro Freestyle 3D scanner. A total of three scans were collected for each vehicle interior to capture all aspects of the interior geometry that must be adjusted in the SVM (Figure 1). The first scan was gathered from the back-middle seat to capture the instrument panels, center console, front of the steering wheel, and roof. The second scan was gathered from the passenger seat to capture the left front door, right side of the steering wheel and column, a-pillar, b-pillar, and driver's seat. The third scan was gathered from outside the left front door to capture the floorpan, foot pedals, left side of the steering wheel, left side of the left instrument panel, and left side of the center console. Prior to scanning, the seat of the exemplar vehicle was adjusted to approximate the recorded position in the CIREN database.

Figure 1. Exemplar vehicle scans from the back-middle seat (left), passenger seat (center), and left door (right) for the Murano reconstruction.

The three 3D scans were processed to generate a shell representing the geometry of the exemplar vehicle scan. The shell was imported into LS-PrePost and aligned to the SVM by approximating the location and orientation of the floor. Each part of the SVM was rigidly transformed in LS-PrePost using translation and rotation until it closely approximated the geometry of the same part of the exemplar vehicle shell (Figure 2). The SVM used in the reconstructions was designed by Iraeus et al. and is the average of 14 different vehicle interiors (Iraeus, 2016). For the Lexus case, the knee bolster airbag developed by Ye, et al. was represented by a low density foam block attached to the SVM knee bolster (Figure 3) (Ye, 2018).

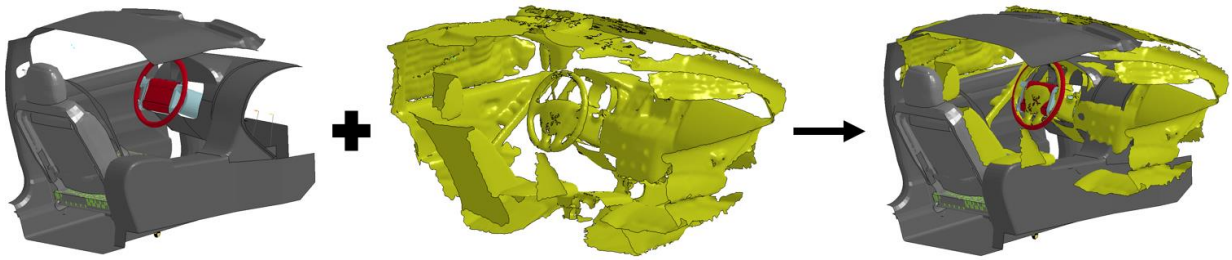

Figure 2. Aligning of the SVM (left) with the exemplar shell (center); following alignment, the individual pieces of the SVM were rigidly translated and rotated to approximate the interior geometry of the exemplar shell.

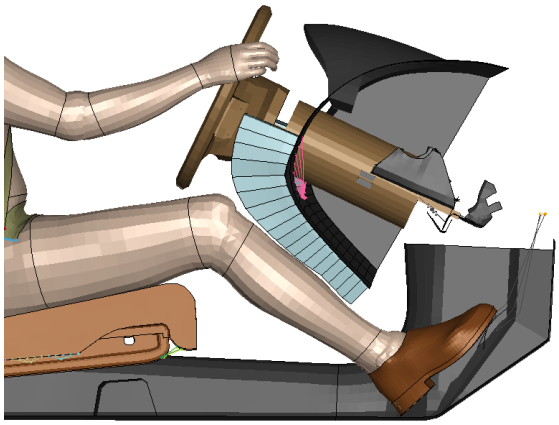

Figure 3. Knee bolster airbag in SVM.

Step 2: HBM Scaling, Positioning, and Belting. The seated simplified 50th percentile male GHBMC v1.8.4.1 human body model was used for the reconstructions. Scaling of the GHBMC was performed with respect to height and mass. Eqs. 1-3 were used to generate a scaling factor, which was used to isometrically scale the GHBMC along the X, Y, and Z-axes (Ye, 2018). Following scaling, the GHBMC was translated and rotated until it was positioned above the SVM seat without creating any initial penetrations. If the HBM did not fit properly into the SVM, the SVM seat was adjusted until the HBM was able to fit. During crash investigations, the current location and posture of the case vehicle seat is recorded, but it is not entirely reliable due adjustments that may have occurred between the crash and the crash investigation.

$$\text{height factor} = \frac{\text{case occupant height}}{\text{GHBMC model height}} \tag{1}$$

$$\text{mass factor} = \sqrt[3]{\frac{\text{case occupant mass}}{\text{GHBMC model mass}}} \tag{2}$$

$$\text{scale factor} = \frac{\text{height factor} + \text{mass factor}}{2} \tag{3}$$

Settling of the GHBMC involved subjecting the entire simulation to a gravitational force of 7.85 N in the Z-axis direction and -4.90 N in the X-axis direction while moving the extremities to the proper location. During settling, the SVM was held in place using boundary prescribed motion of the floor with zero curves for translation and rotation in the X, Y, and Z-axis directions. This allowed for movement of the HBM and the seat without movement of the rest of the SVM. Positioning of the upper extremities was performed by applying a prescribed displacement vector to each hand that was defined from the ventral surface of the head of the 2nd metacarpal bone to the 10 o'clock and 2 o'clock positions of the steering wheel. For the lower extremities, a prescribed displacement vector was applied in the Z-axis direction to the shoe and defined from the back of the heel to the floor of the driver compartment floorpan. All adjustments were conducted in a 300 ms settling simulation. Application of the 3-point belt restraint was performed in LS-PrePost. It was assumed that case occupants were properly belted.

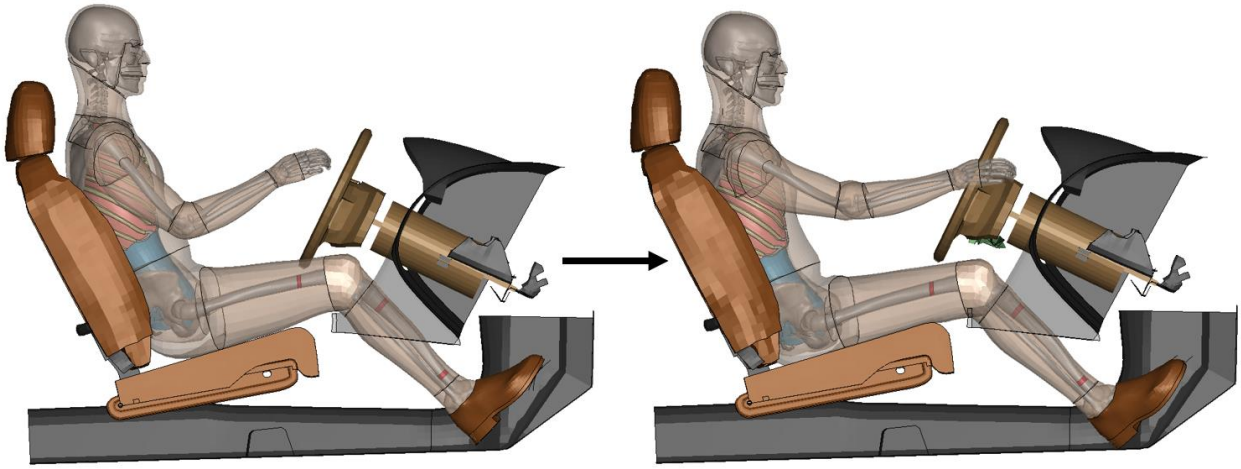

Figure 4. Settling and limb placement of the GHBMC in the SVM.

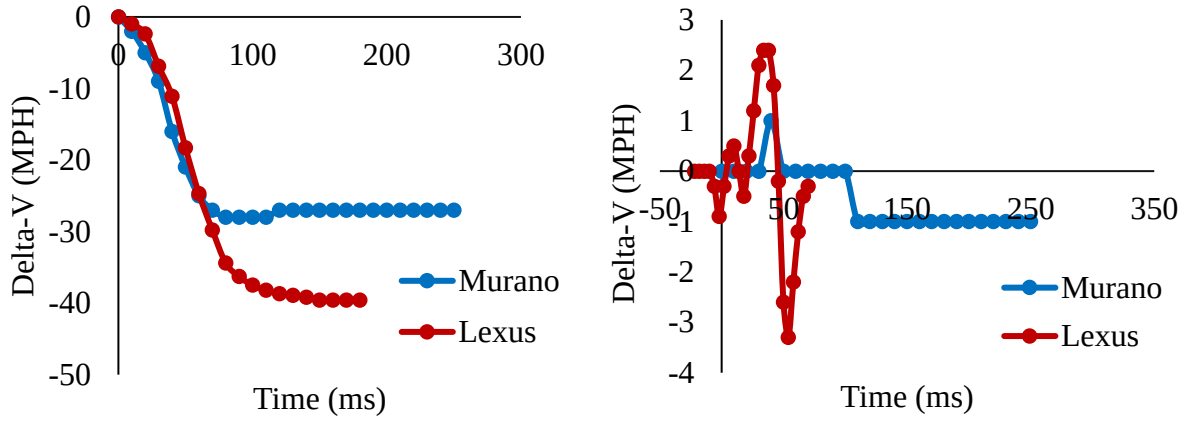

Figure 5. Longitudinal (left) and lateral (right) delta-V curves from the Murano and the Lexus case vehicle EDR reports.

Step 3: Crash Simulation. The longitudinal and lateral delta-V crash pulse curves from the EDR report were applied as boundary prescribed velocities to the floor of the SVM (Figure 5). Rotation was ignored, as it is impossible to determine from the EDR report alone. Airbag deployment and belt pretensioner actuation times were also determined from the EDR report and imported into the simulation. Simulation length was determined by the length of the delta-V curves recorded by the EDR.

Data Analysis

Post-simulation analysis for each crash involved an analysis of occupant kinematics, a comparison of mean integration point maximum principal strain magnitude and location for the ribs and the sternum of the reconstruction HBM and locations of fracture in the case occupant, and an analysis of the usefulness of reconstructions in determining injury causation. Kinematic analysis was done by comparing contact points within the driver compartment between the CIREN case and the reconstruction. The rib and sternum fractures for each case occupant were found using computed tomography (CT) scans of the chest that were collected during initial admission to the hospital. For each fracture, the approximate location was determined in the GHBMC. Maximum strain and time of maximum strain for each fractured rib was determined, in addition to the relative strain in high-strain regions compared to the rest of the bone. A Python script was used to extract the pressure between occupant-to-vehicle contacts so that it would be easy to visualize points of contact throughout the course of the simulation. This information was used to determine times of maximum engagement with the belt and airbag and assist in the determination of injury causation.

RESULTS

Kinematics. In the Murano case, potential contact points include the torso to the steering wheel airbag and belt restraint, the pelvis to the seat pan, and the right knee to the right side of the left knee bolster. The HBM in the Murano reconstruction experienced contact for all of these points. For the Lexus case, there was evidence of potential contact between the torso and the steering wheel airbag, belt restraint, and steering wheel, between the left hand and the left side of the windshield, between the right knee and the right side of the left instrument panel, between the pelvis and the seat pan, between the right hand and the rear-view mirror, and between the right hip and the center console. Similar to the HBM in the Murano reconstruction, the Lexus HBM captures the contacts to the belt restraint, steering wheel airbag, seat pan, and left instrument panel. It also captures contact between the right hand and the A-pillar, near the location of contact on the windshield.

Fractures. Both reconstructions generated elevated strains in the local rib and sternum regions where fracture occurred in the CIREN occupants, especially for ribs 8-9 and the sternum in the Lexus reconstruction. Both reconstructions illustrated elevated strains in the ribs and sternum underneath the path of the belt restraint. The Murano case occupant sustained right 8th and 9th rib fractures and a sternum fracture. Focal points of strain are shown in Figure 7. Average maximum principal strains in regions of fracture were 0.54%, 0.66%, and 1.04% for ribs 8 and 9 and the sternum, respectively. Relative to the unfractured regions, strains were 36.2%, 89.7%, and

39.8% higher in ribs 8 and 9 and the sternum, respectively. The Lexus case occupant sustained fractures of left ribs 3-5, 8, and 9 and a sternal fracture. Focal points of strain for the Lexus case occupant are shown in Figure 8. Average maximum principal strains in regions of fracture were 1.58%, 0.60%, 0.60%, 0.83%, 2.03, and 3.09% for ribs 3-5, 8-9, and the sternum, respectively. Relative to the unfractured regions, strains were 81.8%, 34.2%, 65.2%, 113.3%, 347.1%, and 357.8% higher in ribs 3-5, 8-9, and the sternum, respectively.

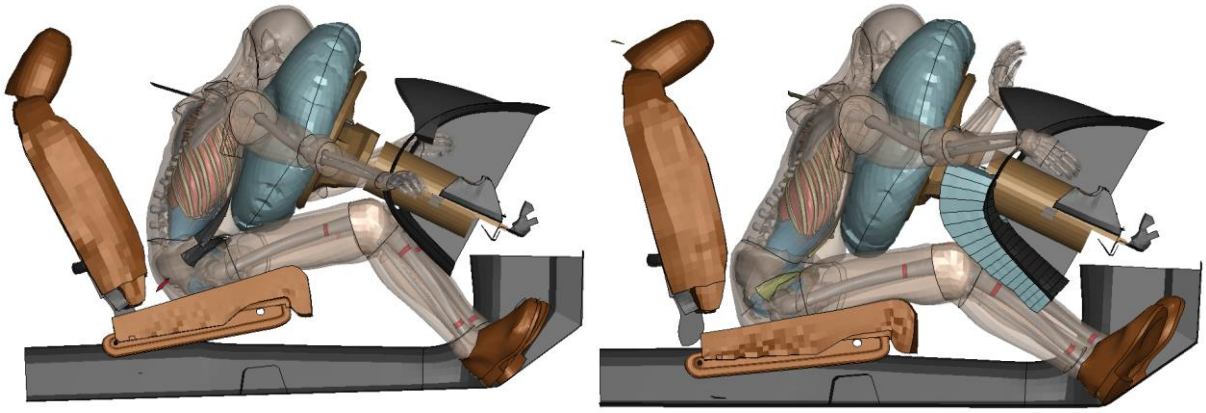

Figure 6. Maximum occupant displacement in the Murano (left) and Lexus (right) reconstructions.

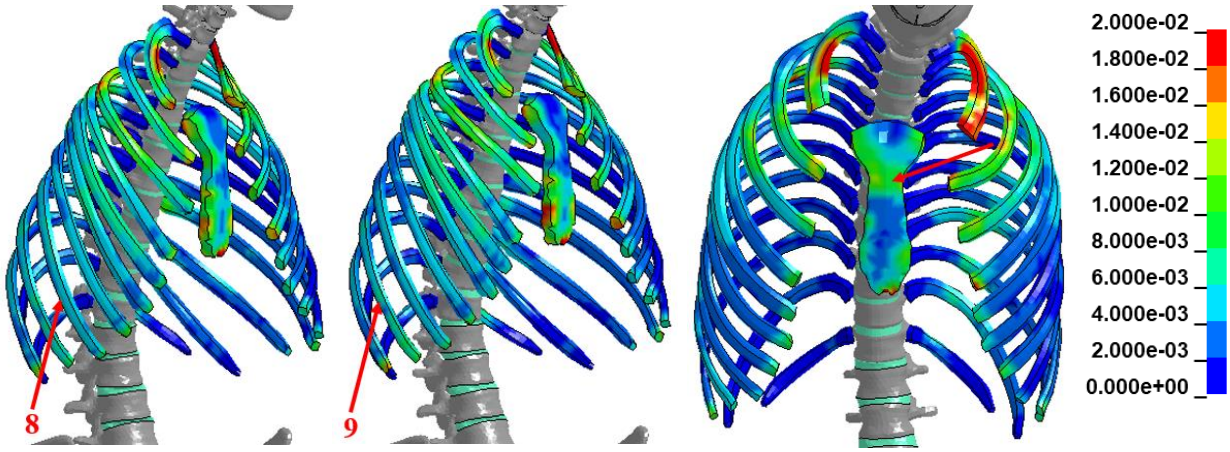

Figure 7. From left to right, maximum strains for the Murano case reconstruction in right lateral rib 8 (time 62.5 ms), right lateral rib 9 (time 57.5 ms), and the sternum (time 85.0 ms). Red arrows indicate approximate location of fracture in case occupant. Strain levels are given on the far right.

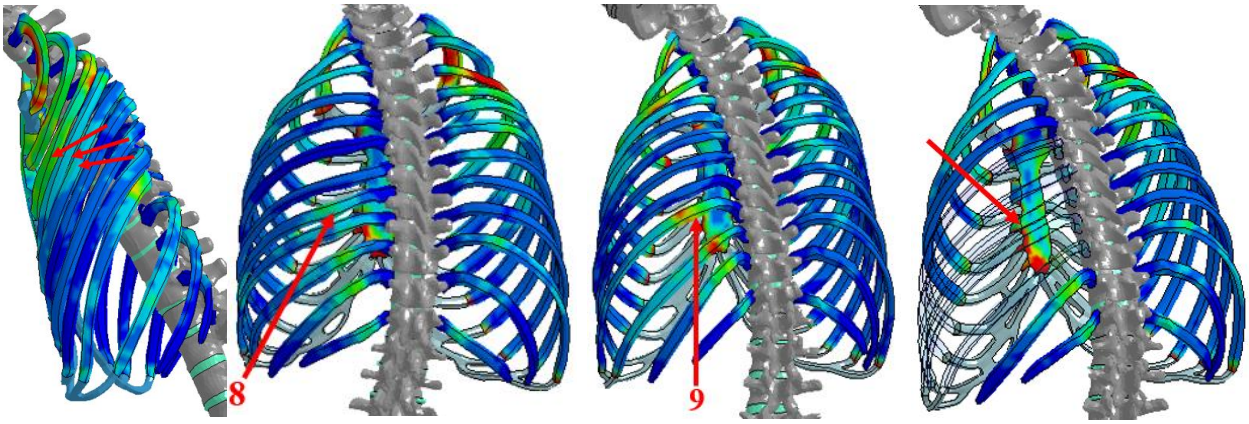

Figure 8. From left to right, maximum strains for the Lexus case reconstruction in left lateral ribs 3-5 (time 97.5 ms), left posterior rib 8 (time 72.5 ms), left posterior rib 9 (time 92.5), and the sternum (time 75.0 ms). Red arrows indicate approximate location of fracture in case occupant. Strain levels are given in Figure 7.

Injury Causation. In both cases, the Python contact viewer allowed for the visualization of contact pressures with the belt restraint, the airbag, and the seat, as well as the approximate time of maximum engagement with each. In the Murano reconstruction, the approximate times of maximum engagement for the belt and airbag were 50 and 85 ms, respectively (Figure 9). In the Lexus reconstruction, the approximate times of maximum engagement for the belt and airbag were 70 and 97.5 ms, respectively. Additionally, because the HBM did not proceed through the airbag and contact the steering wheel in the Lexus reconstruction, there was no evidence of steering wheel contact on the contact viewer. The times of maximum strain in the ribs and sternum occurred around the times of maximum contact engagement of the seatbelt or airbag, allowing for the discernment of which component provided the largest contribution to injury.

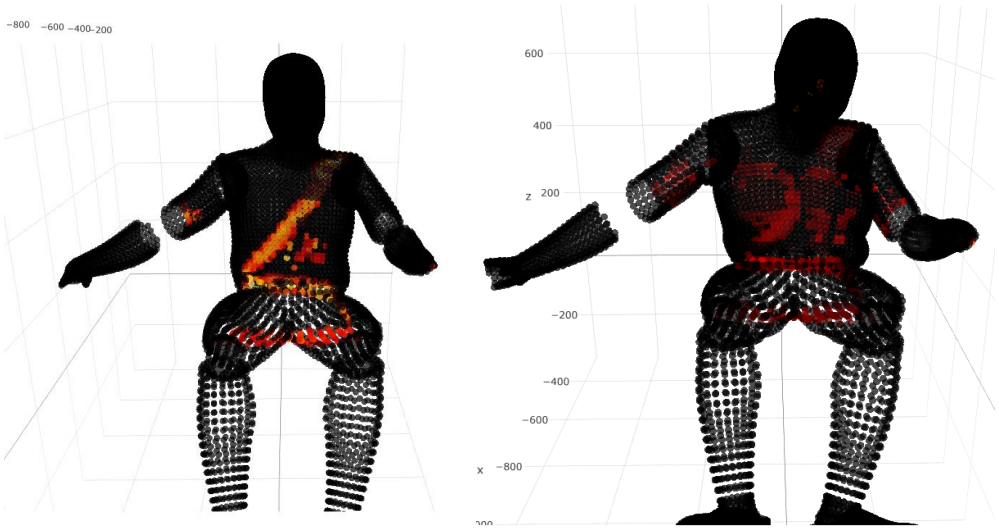

Figure 9. Time of maximum belt and airbag engagement for the Murano reconstruction using Python contact viewer. Maximum belt engagement (left) occurred at approximately 50 ms and maximum airbag engagement (right) occurred at approximately 85 ms.

DISCUSSION

When analyzing the kinematic accuracy of the reconstructions, it is helpful to have as many documented contacts as possible in the case report. For the Murano case, there were only 4 contacts, and each was extremely likely to occur in any frontal collision. The Lexus case report reveals many more contact points, allowing for a more extensive investigation of the accuracy of the reconstruction. When considering thoracic injuries, occupant chest displacement is one of the most important parameters. In the Lexus case, there is strong evidence of steering wheel contact, but the reconstruction does not reflect this. However, for the Murano case, there is no evidence of steering wheel loading, so the chest-to-steering wheel distance is likely more accurate for that reconstruction. Kinematics for the upper extremities are more difficult to gauge, as small changes, such as hand location on the steering wheel, can generate large kinematic differences. For the Lexus reconstruction, the right hand of the HBM contacted the center instrument panel, as opposed to the rear-view mirror, but contact with the rear-view mirror may have occurred if the HBM's hand started in a higher position on the steering wheel.

The reconstructions demonstrated elevated strains in regions of rib and sternum fracture and in regions of belt loading. To assess for risk of fracture, an ultimate strain threshold of 1.8%, as defined by Kent et al., was used (Kent, 2005). Kent et al. used this value for the failure strain of the ribs of older individuals in a FE HBM. Only strains in rib 9 and the sternum for the Lexus reconstruction surpassed this threshold with values of 2.1% and 3.3%, respectively. Kemper et al., in a study of the experimental properties of the ribs from 6 human cadavers, determined an ultimate strain of 2.7%, but this was dependent upon sex, age, bone mineral density, and location on the rib (Kemper, 2005). Forman and Kent defined an equation for determining ultimate strain at any age based upon measurements obtained by Kemper et al. and Carter and Spiegler (Carter, 1978; Forman, 2012; Kemper, 2005; Kemper, 2007). Though more precise fracture thresholds exist, the threshold defined by Kent et al. was chosen due to its simplicity. When fracture risk is not considered, the reconstructions are still valuable in that they display focal regions of strain in areas of fracture.

When used with the Python contact viewer, the reconstructions display the ability to assist in the determination of injury causation. The shoulder belt, steering wheel, and steering wheel airbag are the three main components associated with rib fractures in frontal collisions (Bansal, 2011). By knowing the times of maximum shoulder belt and airbag engagement and correlating it with the time of maximum strain for regions of fracture, a more informed decision of injury causation is established. Belt-only restraint systems are associated with more fractures than belt and airbag restraint systems (Crandall, 2000; Kallieris, 1998). Additionally, in a study of older adults, Bansal et al. determined that rib and sternum fractures are most commonly caused by the shoulder belt, as opposed to the airbag and steering wheel (Bansal, 2011). When it comes to the coding of injuries in CIREN, this does not mean that the belt or the airbag will be determined as the sole component responsible for fracture. Instead, the relative contribution of each component will be determined. For example, since the belt will nearly always be the main culprit involved in rib and sternum fractures of belted occupants, the confidence involved with airbag contribution may increase or decrease based upon reconstruction results (Schneider, 2011).

LIMITATIONS

The main two limitations to this study are associated with unknown details within each CIREN case. When determining contact points in CIREN cases, it is often difficult to determine whether scuffs, dents, and other evidence of contact are the result of contact by the occupant or some other object that was loose in the vehicle. Additionally, it may be difficult to discern what region of the occupant's body was associated with the contact. For these reasons, there may be minimal contact points, as in the Murano case, or reported contact points may be inaccurate. When transforming the vehicle seat, it is difficult to determine the seat positioning and angle. It is possible that the seat is adjusted between the time of the crash and when the crash investigator inspects it. Seat location and orientation are considered when obtaining exemplar scans and transforming interior geometries, but there are still many unknowns and, often, the seat location and orientation of best fit is used.

FUTURE WORK AND APPLICATIONS

Future directions for the study include measures that will allow the reconstructions to be generalized to a large variety of MVCs. The implementation of a side airbag would allow for near side crashes to be reconstructed. The inclusion of intruding components would also allow a significantly greater range of applications. Injury metrics will also be implemented, to allow for more extensive injury analysis and to aid in the determination of injury causation. For example, Gaewsky et al. used combined thoracic index to assess for the risk in developing thoracic injuries, such as a hemomediastinum, and head injury criteria to assess for the risk in developing brain injuries, such as intraparenchymal hemorrhage (Gaewsky, 2015).

CONCLUSIONS

CIREN case reconstructions involving finite element human body models provide greater insight into crash kinematics and injury causation for specific CIREN cases. Rib and sternum injuries in case occupants were correlated with regions of strain in reconstructions, caused by belt and airbag loading. Reconstructions were able to discern times of maximum belt restraint and airbag engagement, thereby allowing for greatly improved determination of injury causation in frontal collisions. With continued improvement, these reconstructions can become an extremely valuable tool for CIREN case reviews and be adapted to multiple collision types.

REFERENCES

Bansal, V., Conroy, C., Chang, D., Tominaga, G. T., & Coimbra, R. (2011). Rib and sternum fractures in the elderly and extreme elderly following motor vehicle crashes. Accid Anal Prev, 43(3), 661-665.

Belwadi, A., Siegal, J. H., Singh, A., Smith, J. A., Yang, K. H., & King, A. I. (2012). Finite element aortic injury reconstruction of near side lateral impacts using real world crash data. J Biomech Eng, 134(1).

Carter, D. R., & Spengler, D. M. (1978). Mechanical properties and composition of cortical bone. Clin Orthop Relat Res, 135, 192-217.

Crandall, J., Kent, R., Patrie, J., Fertile, J., & Martin, P. (2000). Rib Fracture Patterns and Radiologic Detention - A Restraint-Based Comparison. Annu Proc Assoc Adv Automot Med, 44, 235-260.

Danelson, K. A., & Stitzel, J. D. (2015). Finite element model prediction of pulmonary contusion in vehicle-to-vehicle simulations of real-world crashes. Traffic Inj Prev, 16(6), 627-636.

Forman, J. L., & Kent, R. W. (2012). Predicting rib fracture risk with whole-body finite element models: development and preliminary evaluation of a probabilistic analytical framework. Ann Adv Automot Med, 56, 109-124.

Gaewsky, J. P., Weaver, A. A., Koya, B., & Stitzel, J. D. (2015). Driver injury risk variability in finite element reconstructions of Crash Injury Research and Engineering Network (CIREN) frontal motor vehicle crashes. Traffic Inj Prev, 16(sup2), S124-S131.

Hayashi, S., Yasuki, T., & Kitagawa, Y. (2008). Occupant kinematics and estimated effectiveness of side airbags in pole side impacts using a human FE model with internal organs. Stapp Car Crash J, 52, 363-377.

Iraeus, J., & Lindquist, M. (2016). Development and validation of a generic finite element vehicle buck model for the analysis of driver rib fractures in real life nearside oblique frontal crashes. Accid Anal Prev, 95(Pt A), 42-56.

Kallieris, D., Conte-Zerial, P., Rizzetti, A., & Mattern, R. (1998). Prediction of thoracic injuries in frontal crashes. Paper 98-S7-O-04. Proc. ESV.

Kemper, A. R., McNally, C., Kennedy, E. A., Manoogian, S. J., Rath, A. L., Ng, T. P., . . . Duma, S. M. (2005). Material properties of human rib cortical bone from dynamic tension coupon testing. Stapp Car Crash J, 49, 199-230.

Kemper, A. R., McNally, C., Pullins, C. A., Freeman, L. J., Duma, S. M., & Rouhana, S. M. (2007). The biomechanics of human ribs: material and structural properties from dynamic tension and bending tests. Stapp Car Crash J, 51, 235-273.

Kent, R., Lee, S. H., Darvish, K., Wang, S., Poster, C. S., Lange, A. W., . . . Matsuoka, F. (2005). Structural and material changes in the aging thorax and their role in crash protection for older occupants. Stapp Car Crash J, 49, 231-249.

Newman, R. J., & Jones, I. S. (1984). A prospective study of 413 consecutive car occupants with chest injuries. J Trauma, 24(2), 129-135.

Schneider, L. W., Rupp, J. D., Scarboro, M., Pintar, F., Arbogast, K. B., Rudd, R. W., . . . Eppinger, R. (2011). BioTab - a new method for analyzing and documenting injury causation in motor-vehicle crashes. Traffic Inj Prev, 12(3), 256-265.

Shigeta, K., Kitagawa, Y., & Yasuki, T. (2009). Development of next generation human FE model capable of organ injury prediction. Proceedings of the 21st Annual Enhanced Safety of Vehicles.

WHO. (2018). *Global Status Report on Road Safety*. Retrieved from France:

Ye, X., Gaewsky, J. P., Jones, D. A., Miller, L. E., Stitzel, J. D., & Weaver, A. A. (2018). Computational modeling and analysis of thoracolumbar spine fractures in frontal crash reconstructions. Traffic Inj Prev, 19(sup2), S32-S39.